Interactions of the chemotaxis signal protein CheY with bacterial flagellar motors visualized by evanescent wave microscopy

Shahid Khan*, Daniel Pierce†‡ and Ronald D. Vale†

The chemotaxis signal protein CheY of enteric bacteria shuttles between transmembrane methyl-accepting chemotaxis protein (MCP) receptor complexes and flagellar basal bodies [1]. The basal body C-rings, composed of the FliM, FliG and FliN proteins, form the rotor of the flagellar motor [2]. Phosphorylated CheY binds to isolated FliM [3] and may also interact with FliG [4], but its binding to basal bodies has not been measured. Using the chemorepellent acetate to phosphorylate and acetylate CheY [5], we have measured the covalent-modification-dependent binding of a green fluorescent protein–CheY fusion (GFP–CheY) to motor assemblies in bacteria lacking MCP complexes by evanescent wave microscopy [6].
At acetate concentrations that cause solely clockwise rotation, GFP–CheY molecules bound to native basal bodies or to overproduced rotor complexes with a stoichiometry comparable to the number of C-ring subunits. GFP–CheY did not bind to rotors lacking FliM/FliN, showing that these subunits are essential for the association. This assay provides a new means of monitoring protein–protein interactions in signal transduction pathways in living cells.

Addresses: *Laboratory of Cellular Bioenergetics, Department of Physiology and Biophysics, Albert Einstein College of Medicine, Bronx, New York 10461, USA. †Howard Hughes Medical Institute and Department of Cellular and Molecular Pharmacology, University of California, San Francisco, California 94143, USA.

‡Present address: Departments of Chemistry and Biochemistry, Montana State University, Boseman, Montana 59717, USA.

Correspondence: Shahid Khan
E-mail: skhan@aecom.yu.edu.

Received: **27 April 2000**
Revised: **12 June 2000**
Accepted: **12 June 2000**

Published: **21 July 2000**

Current Biology 2000, 10:927–930

0960-9822/00/$ – see front matter

Results and discussion

To measure CheY–motor interactions we used an evanescent wave microscope [6]. First, we constructed a functional GFP–CheY fusion. In swarm assays on semi-solid agar, this complemented the *Escherichia coli cheY* deletion mutant KO641 [7] at levels comparable to the wild-type CheY protein when both were expressed under *araBAD* control [8]. Second, we used the membrane-permeable weak-acid chemorepellent acetate to induce dual covalent modification of GFP–CheY. Acetate effects CheY phosphorylation and acetylation by enzymatic reaction [5], unlike most chemotactic stimuli that bind to a MCP and modulate CheY phosphorylation activity of the MCP-associated CheA kinase [1]. We could thus measure modification-dependent association of GFP–CheY with flagellar motor components in *E. coli* lacking MCPs. Finally, we overproduced *Salmonella typhimurium* rotor complexes so that up to 200 complexes were assembled in the cytoplasmic membranes of host *E. coli* [9], a level 30-fold greater than that present in motile *S. typhimurium*/*E. coli*. Rotors with intact or partial C-rings respectively were assembled upon co-expression of the integral membrane protein FliF with FliG, FliM and FliN, or FliG alone (Figure 1a). Bacteria were attached to the coverslide surface and GFP fluorescence was excited by the evanescence wave created by total internal reflection of an argon-ion laser beam. The intensity, I_{ex}, of the excitation evanescent wave varies exponentially with distance, z, from the coverslide surface; $I_{ex} = I_{ex(z=0)} \exp(-z/d)$ [10], where d depends on wavelength, incidence angle and refractive index difference (Figure 1b). Thus, we could monitor local GFP–CheY concentration near the cell wall attached to the coverslide without exciting the bulk of the cytoplasmic GFP–CheY, thereby greatly reducing the background signal.

Evanescent wave microscope images of RBB1050 *E. coli* [7] expressing GFP–CheY in acetate buffer revealed punctate spots (Figure 2a,b). The size of these spots was diffraction limited, as determined by comparison of the images with those of single, surface-adsorbed GFP molecules fused with a monomeric mutant kinesin (data not shown). The number of spots per cell image was consistent with the number of flagella per cell (6.6 ± 1.4 [11]) (Figure 2a), given that half of each cell was imaged (Figure 1b). The punctate distribution was not observed when GFP–CheY was expressed in an isogenic, non-flagellate strain (RP3098 [12]) lacking all flagellar and chemotaxis proteins (Figure 2c) or in the C41 strain [13] used for protein expression. We infer that the spots represent GFP–CheY molecules associated with motors. To estimate the number of GFP–CheY molecules bound per C-ring, the RBB1050 cell background was subtracted from the spot intensities, which were then compared with the mean single-molecule GFP intensity, after correction for camera sensitivity and integration times (Figure 2 legend). Accuracy of the comparison was limited by uncertainty in z. Given that the cell wall flattens upon attachment by the antibodies to the coverslide, z could be as small as 35 nm

Figure 1

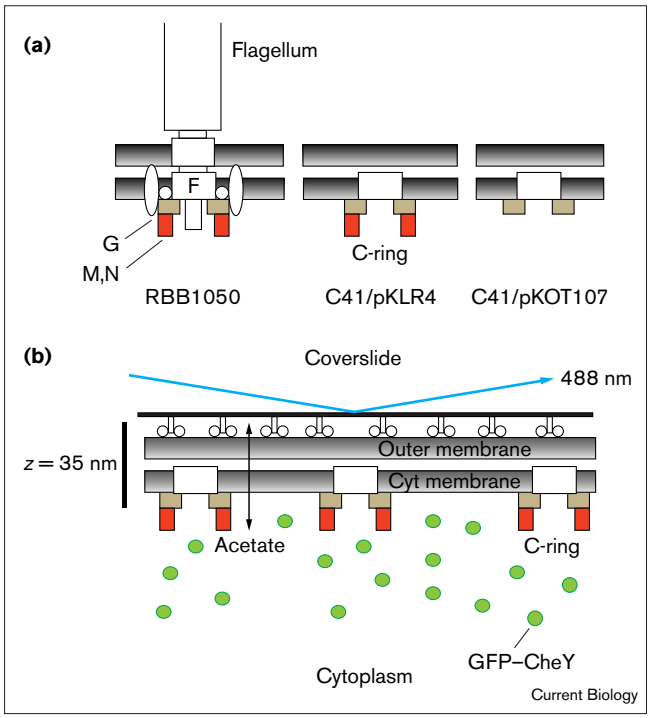

Evanescent wave microscope assay for interactions between CheY and the flagellar motor. **(a)** Flagellar motor complexes in the *E. coli* strains used. RBB1050 (*tsr*$^-$, *tar*$^-$, *tap*$^-$, *trg*$^-$, *cheA*$^-$, *cheW*$^-$, *cheB*$^-$, *cheR*$^-$, *cheY*$^-$, *cheZ*$^-$) [7] has functional flagella but cannot form MCP receptor complexes or adapt to acetate-induced GFP–CheY modification. In native basal bodies, as in RBB1050, FliG (G, brown) and FliM (M, red) are present in approximately equimolar ratio and copy numbers sufficient to form a single circumferential array of diameter 45 nm, the size of the C-ring. FliG is adjacent to FliF (F) whereas assembly of FliM and FliN (N, red) into the C-ring is coupled [2]. Ellipses denote transmembrane stator MotA–MotB complexes whose interactions with FliG generate torque [19]. Basal bodies also contain proteins required for flagellar protein export (rectangle) and of unknown function (circles) (see [9]). C41 is a non-flagellate BL21(λDE3) derivative used for protein over-expression [13]. pKLR4 expresses *S. typhimurium* FliF, FliG, FliM and FliN. It was constructed from pKLR3 [9] by moving the genes from the multiple cloning site of pKLR3 to pET23. pKOT107 expresses *S. typhimurium* FliF and FliG [17]. **(b)** Bacteria expressing GFP–CheY were attached to the coverslide by antibodies against *E. coli* outer membranes. *Mut1–gfp* [20] was fused to *E. coli cheY* by a proline-rich polylinker by PCR and moved into pSU19 [9] and pBAD33 [8], giving pKLR5 and pKFK2, respectively. Control bacteria lacking GFP–CheY could not be visualized. C-rings protrude 17 nm into the cytoplasm [15] and, upon overproduction, packed cytoplasmic membranes with a mean separation of 150 nm. $z = 35 \pm 8$ nm for C-ring CheY-binding sites, given a 22 nm thick cell wall [21] and a 5 nm antibody layer. F_{lens}, is estimated [22] as ~400 nm for the objective (100×, 1.4 numerical aperture) used. $d = 96$ nm for 488 nm wavelength, 78° incidence and refractive indices 1.47 and 1.38 for fused silica and *E. coli* cytoplasm [23], respectively. Refractive indices of prism, glycerol and coverslide were matched. I_{ex} is 0.7 and 0.015 times I_{ex} at the coverslide–sample interface ($z = 0$) for $z = 35$ and 400 nm, respectively.

for C-rings (Figure 1). This yields an estimate of 22 GFP–CheY molecules per motor, with ±20% sampling error. In the absence of deformation, z will be greater as a result of cell curvature. For an ideal cylinder, it will be ~100 nm for C-rings at a horizontal distance half a cell radius away from the cell center. The estimated GFP–CheY per motor will increase correspondingly to 37. The actual value will lie somewhere between these two extremes.

When tethered by a single flagellum to a glass coverslip, RBB1050 *E. coli* expressing GFP–CheY under *lac* control (pKLR5) rotated exclusively clockwise in 30 mM acetate, but predominantly counterclockwise in its absence, as seen previously in other strains lacking chemotaxis proteins [14]. The change was rapid (a few seconds) upon addition of acetate in a flow-cell. In the absence of acetate, no GFP–CheY spots were generally detectable in RBB1050 cells. We therefore used cells overproducing rotor complexes, which also enabled evaluation of the role of motor components and other basal body proteins.

Rotor proteins and GFP–CheY were expressed from two compatible plasmids. Bacterial cultures were harvested, divided into two and resuspended in assay buffer with or without acetate. The evanescent wave fluorescence from cells in the presence of acetate was 1.94 ± 0.05 times more intense than from control cells without acetate (Figure 3). This increase indicated the association of GFP–CheY with membrane-bound C-rings. The roughly twofold increase was similar to the ratio of the intensity of the punctate spots relative to background in RBB1050 cells. Acetate had no effect when the experiment was repeated with cultures expressing GFP–CheY alone. Furthermore, the population-averaged evanescent wave fluorescence from cells expressing GFP–CheY alone was similar to that from cells expressing GFP–CheY with rotor complexes in the absence of acetate. Therefore, given the culture-to-culture variation, the binding of unmodified GFP–CheY to rotors could not be resolved.

In the overproduction system, the number of GFP–CheY molecules bound per rotor may be estimated if intracellular GFP–CheY concentration is known. Intracellular GFP–CheY in these experiments, determined from triplicate immunoblot measurements using CheY protein standards and affinity-purified antibodies, was $25{,}000 \pm 5000$ copies per cell. C-rings localize in a layer of cytoplasm 20 nm deep adjacent to the cytoplasmic membrane. In the absence of binding to C-rings, the number of GFP–CheY molecules in this layer excited by the evanescent wave will be $(25{,}000 \times 20a)/V_c$, where V_c is cell volume and a the area of the membrane proximal to the coverslide. The corresponding number of rotors will be $200a/A_c$, where A_c is cell area. Therefore, the unbound GFP–CheY per rotor ratio, R_{free}, is $2500/(V_c/A_c) = 2500/\{(\pi r^2 l + (4/3)\pi r^3)/(2\pi r l + 4\pi r^2)\} = 9.3$ for an average *E. coli* cell approximated as a cylinder of length $l = 2$ μm and radius $r = 0.5$ μm, with hemispherical end-caps. The fluorescence intensity per

Figure 2

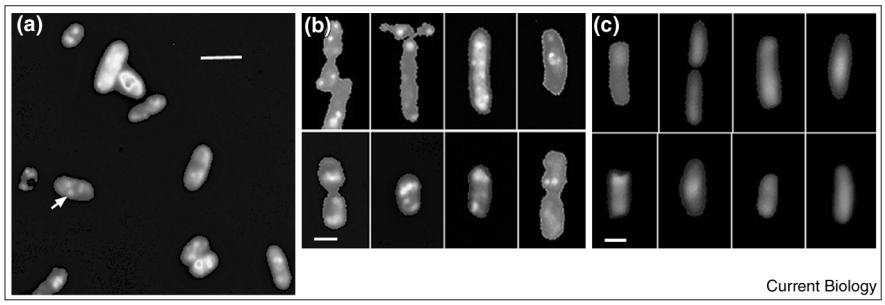

Evanescent wave excited fluorescence images of GFP–CheY in *E. coli*. **(a)** Low-magnification image of immobilized RBB1050/pKLR5 in acetate assay buffer (30 mM sodium acetate/20 mM potassium phosphate pH 7.0, 50 mM sodium chloride, 10 mM lithium lactate, 100 μM EDTA), showing GFP–CheY spot clusters (arrow indicates an example). There are 2.9 ± 1.5 spots per cell image. Scale bar represents 2 μm. Single cell images of **(b)** RBB1050/pKLR5 and **(c)** RP3098/pKLR5. Scale bars represent 1 μm. The images were acquired using a digital CCD camera (SensiCam II, Cooke Corporation) with a 1280 × 1280 pixel array. Acquisition times were typically 2–5 s. The cell images were compared with four-frame averaged video images of surface-adsorbed ($z = 0$) GFP–Kin339 molecules [20], acquired on the same microscope using a Stanford Photonics ICCD/Hamamatsu Argus 20 image processor as previously described [6]. A moveable mirror directed the emitted fluorescence onto one or the other camera. The videotaped images were digitized using a frame grabber card (I/O-702; InSync Technologies). The excitation laser beam was adjusted to be in the range where its modulation by neutral density filters resulted in a proportionate change in image intensity. Images of the same field of RP3098 cells taken by both cameras were used to compare pixel magnification and intensities. The diffraction-limited spot intensities were measured by point integration over a square pixel array equal to the spot size (SigmaScan Image Morphometric Analysis Software). Gray levels of the images shown have been stretched to enhance contrast.

unit image area (I_{em}) recorded for each cell is: $I_{em} = kC\Sigma I_{ex}(z = 25\ nm - F_{lens})$ where C is GFP–CheY concentration, F_{lens} the depth of field, and k the I_{em}/I_{ex} ratio at the coverslide sample interface ($z = 0$) and unit concentration. The fraction of the total fluorescence contributed by GFP–CheY molecules in the 20 nm layer adjacent to the membrane is 19.2% when GFP–CheY concentration is uniform throughout the cell. If the acetate-dependent 1.94-fold increase in I_{em} arises solely from binding of GFP–CheY to C-rings, the relative concentration increase in this layer is $\{(1.94 - (1 - 0.192))/0.192\} = 5.9$-fold. Therefore, the ratio of bound GFP–CheY per rotor, $R_{bound} = (5.9 - 1) \times 9.3 = 45$. The calculation assumes that free GFP–CheY concentration does not change upon binding. Saturation occupancy of all 200 rotor FliM subunits will result in a 28% decrease in free GFP–CheY, increasing R_{bound} by the same fraction. R_{free} and, thus, R_{bound} are independent of the extent of the cell imaged by the evanescent wave. R_{bound} is also insensitive to z because it is obtained by measurement of a relative intensity increase, normalized for sample geometry. It is, however, sensitive to the location of the C-ring CheY-binding sites relative to the membrane and to the cytoplasmic refractive index. Uncertainty in these parameters converts to a 20% error in the fractional decrease in I_{ex} during penetration through the 20 nm cytoplasmic layer. Given similar errors for the immunoblot determinations of cellular GFP–CheY and rotor proteins, the cumulative error in the estimate of R_{bound} is 40%.

The number of GFP–CheY molecules bound per rotor, as estimated by two independent methods subject to different assumptions and errors, was 22–37 for native basal bodies and 57 ± 23 for overproduced rotors. These estimates are similar to those for the numbers of C-ring subunits (34 ± 1 [15]) and FliM copies per flagellum (33.7 ± 5.5 [2]). Therefore, the increase in GFP–CheY occupancy of the rotors, upon covalent modification by acetate at concentrations known to cause complete clockwise rotation, is comparable to the number of rotor subunits. It follows that occupancy in the absence of modification is small, if any.

We next investigated whether FliM was required for association of GFP–CheY with rotors. Bidirectional rotation is restored in clockwise or counterclockwise locked CheY mutants by mutations in FliG as well as in FliM, suggesting potential interaction with both subunits; but the screens used for phenotype identification did not test for chemotaxis [4]. *In vitro*, CheY binds to purified FliM but not to FliG [3]. Both proteins were, however, solubilized from inclusion bodies by urea and refolded by dialysis. Thus, the conclusion that FliG does not bind CheY has the caveat that the denatured/renatured FliG may not have folded into its native conformation. Also, CheY–FliG interaction may be weak *in vitro*, but significant in the cytoplasm as a result of macromolecular crowding [16].

We formed partial rotor complexes in the membrane by expressing FliF and FliG alone [9] and showed by immunoelectron microscopy that these complexes contained both proteins, consistent with reports that FliG binds stoichiometrically to FliF *in vitro* [17]. When acetate was added to cells overproducing partial rotors, no difference in GFP–CheY distribution was observed by evanescent wave microscopy (Figure 3). Thus FliG, even when part of rotor complexes *in situ*, cannot bind CheY in the absence of FliM and FliN.

Figure 3

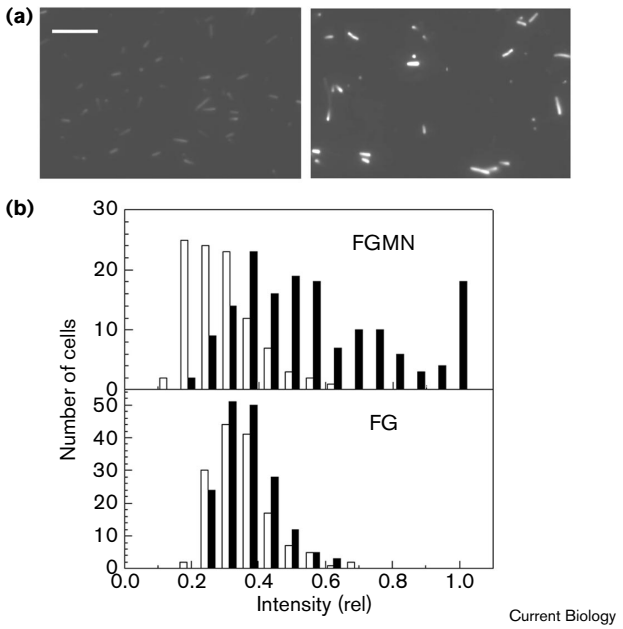

Evanescent wave excited fluorescence from C41/pKLR4/pKFK2 *E. coli* co-expressing GFP–CheY with rotor complexes. **(a)** The effect of acetate. To induce expression of the proteins, isopropylthio-galactoside (IPTG) and L-arabinose were added at 1 mM final concentration to an exponentially growing culture in Luria broth at 30°C, 2 h before harvest, wash and resuspension of the cells in assay buffer (with (left panel) and without (right panel) acetate). Images were obtained over a 20 min period after a ~5 min interval to mount and focus a sample on the microscope (15 min mean acquisition time). The images show fields of bacteria obtained from one such culture in buffer without (left panel) and with (right panel) acetate. Image gray levels have been stretched as in Figure 2. Scale bar represents 20 μm. **(b)** GFP–CheY fluorescence intensity histograms of bacteria overproducing intact (C41/pKLR4/pKFK2) rotors (FGMN) and partial (C41/pKOT107/pKFK2) rotors (FG) in buffer with (black bars) and without (white bars) acetate. Pre-contrast enhanced image intensities were measured by line integration along the long axis of the bacteria. The 4096 gray levels of the digital CCD were binned (64 levels/bin) and plotted as a relative intensity scale where 1 indicates the saturation time-integrated camera readout. Mean cell intensities with (I+) and without (I–) acetate were computed. (I+/I–) ratios were 1.94 ± 0.05 and 1.04 ± 0.04 for intact and partial rotors respectively. A fraction of the population from cultures expressing intact rotors and GFP–CheY in acetate saturated the camera. Correction by spline fit of the distribution increased (I+/I–) by 15%.

In summary, we have found that GFP–CheY bound to rotors in numbers consistent with formation of a stoichiometric complex with C-ring subunits, that binding was controlled by covalent modification, that GFP–CheY bound intact rotor complexes as well as native basal bodies, ruling out a requirement for other flagellar basal body proteins or rotor–stator interactions, and that FliF–FliG complexes did not bind GFP–CheY, consistent with FliM being the binding site for CheY. Our assay provides a real-time method for *in vivo* quantification of weak interactions of cytoplasmic proteins with membrane assemblies that are difficult to study in isolated preparations using biochemical or electron microscopy methods. This approach using evanescent wave microscopy should be a generally valuable tool for mapping intracellular signaling chemistry onto cellular response [18].

References

1. Falke JJ, Bass RB, Butler SL, Chervitz SA, Danielson MA: **The two-component signalling pathway of bacterial chemotaxis: a molecular view of signal transduction by receptors, kinases, and adaptation enzymes.** *Annu Rev Cell Dev Biol* 1997, **13:**457-512.
2. Zhao R, Pathak N, Jaffe H, Reese TS, Khan S: **FliN is a major structural protein of the C-ring in the *Salmonella typhimurium* flagellar basal body.** *J Mol Biol* 1996, **261:**195-208.
3. Welch M, Oosawa K, Aizawa S-I, Eisenbach M: **Phosphorylation-dependent binding of a signal molecule to the flagellar switch of bacteria.** *Proc Natl Acad Sci USA* 1993, **90:**8787-8791.
4. Roman SJ, Meyers M, Volz K, Matsumura P: **A chemotactic signaling surface on CheY defined by suppressors of flagellar switch mutations.** *J Bacteriol* 1992, **174:**6247-6255.
5. Ramakrishnan R, Schuster M, Bourret RB: **Acetylation at Lys92 enhances signaling by the chemotaxis response regulator protein CheY.** *Proc Natl Acad Sci USA* 1998, **95:**4918-4923.
6. Pierce DW, Vale RD: **Single molecule fluorescence detection of green fluorescence protein and application to single molecule dynamics.** *Methods Cell Biol* 1999, **58:**49-73.
7. Abouhamad WN, Bray D, Schuster M, Boesch KC, Silversmith RE, Bourret RB: **Computer-aided resolution of an experimental paradox in bacterial chemotaxis.** *J Bacteriol* 1998, **180:**3757-3764.
8. Guzman L-M, Belin D, Carson MJ, Beckwith J: **Tight regulation, modulation and high-level expression by vectors containing the arabinose ρ_{BAD} promotor.** *J Bacteriol* 1995, **177:**4121-4130.
9. Lux R, Kar N, Khan S: **Overproduced *S. typhimurium* flagellar motor switch complexes.** *J Mol Biol* 2000, **298:**577-584.
10. Axelrod D: **Total internal reflection fluorescence microscopy.** *Methods Cell Biol* 1989, **30:**245-270.
11. Khan S, Dapice M, Reese TS: **Effects of *mot* gene expression on the structure of the flagellar motor.** *J Mol Biol* 1988, **202:**575-584.
12. Smith RA, Parkinson JS. **Overlapping genes at the *cheA* locus of *Escherichia coli*.** *Proc Natl Acad Sci USA* 1980, **77:**5370-5374.
13. Miroux B, Walker JE: **Over-production of proteins in *Escherichia coli*: mutant hosts that allow synthesis of some membrane proteins and globular proteins at high levels.** *J Mol Biol* 1996, **260:**289-298.
14. Dailey FE, Berg HC: **Change in direction of flagellar rotation in *Escherichia coli* mediated by acetate kinase.** *J Bacteriol* 1993, **175:**3236-3239.
15. Thomas DR, Morgan DG, DeRosier DJ: **Rotational symmetry of the C ring and a mechanism for the flagellar rotary motor.** *Proc Natl Acad Sci USA* 1999, **96:**10134-10139.
16. Zimmerman SB, Minton AP: **Macromolecular crowding: biochemical, biophysical and physiological consequences.** *Annu Rev Biophys Biomol Struct* 1993, **22:**27-95.
17. Oosawa K, Ueno T, Aizawa S-I: **Overproduction of the bacterial flagellar switch complex proteins and their interactions with the MS ring complex *in vitro*.** *J Bacteriol* 1994, **176:**3683-3691.
18. Sako Y, Minoghchi S, Yanagida T: **Single molecule imaging of EGFR signalling on the surface of living cells.** *Nature Cell Biol* 2000, **2:**168-172.
19. Lloyd, SA, Whitby FG, Blair DF, Hill CP: **Structure of the C-terminal domain of FliG, a component of the rotor in the bacterial flagellar motor.** *Nature* 1999, **400:**472-476.
20. Case RB, Pierce D, Hom-Booher N, Hart CL, Vale RD: **The directional preference of kinesin motors is specified by an element outside of the motor catalytic domain.** *Cell* 1997, **90:**959-966.
21. Nikaido H, Nakae T: **The outer membrane of gram negative bacteria.** *Adv Microb Physiol* 1979, **20:**163-250.
22. Inoue S: *Video Microscopy*. New York: Plenum Press; 1996.
23. Valkenburg JAC, Woldringh CL: **Phase separation between nucleoid and cytoplasm in *Escherichia coli* as defined by immersive refractometry.** *J Bacteriol* 1984, **160:**1151-1157.